2024 European Control Conference (ECC)
June 25-28, 2024. Stockholm, Sweden

RADAR-Based Safe Pull-Over of Autonomous Racing Cars in Localization Failure Scenarios

Francesco Prignoli, Paolo Falcone, Ayoub Raji, and Marko Bertogna

***Abstract*— This paper presents a RADAR-Based, vehicle lateral dynamics control algorithm that ensures a safe pull-over of autonomous racing vehicles to the roadside barriers in the event of localization failures. The position and curvature of the roadside barriers are estimated from RADAR measurements through a Total Least Squares algorithm and fed to a Linear-Quadratic-Regulator (LQR), which outputs the steering commands to the vehicle. As the estimates accuracy varies with the distance to the barriers, the proposed algorithm controls the car at a target distance which is dynamically adjusted based on the confidence interval of the barrier distance estimate. The convergence of the resulting closed-loop, nonlinear system to a minimum safe distance to the barrier is proven through Lyapunov stability theory. We consider the setup based on the Dallara AV-21, a fully autonomous racing car competing in the Indy Autonomous Challenge. Simulations on the Las Vegas Motor Speedway track demonstrate the emergency controller's effectiveness, offering a robust safety solution for racing cars in case of localization losses.**

I. INTRODUCTION

The quest for enhanced safety and control in the domain of autonomous racing cars has driven the development of sophisticated technologies that enable these high-performance vehicles to operate at the edge of their capabilities. One particular challenge arises in the case of localization failure, which require the design of emergency systems capable of swiftly taking control of the vehicle and executing a safe pull-over. This paper presents the design and implementation of a RADAR-based safe pull over maneuver for autonomous racing cars, with a specific focus on situations involving localization failures, such as GPS signal loss and LiDAR faults. The reference vehicle is the Dallara AV-21, competing in the *Indy Autonomous Challenge*[1]. This fully autonomous racing car boasts an extensive sensor suite encompassing three RADARs, three LiDARs, six cameras, and two dual-antenna GPS-RTK systems. Typically, the primary means of localization relies heavily on GPS [1] [2]; however, even with redundancy measures in place, signal loss can significantly impact these sensor systems, especially in the presence of obstacles like buildings, banners, bridges, and tunnels. For these reasons, emergency routines must be in place to prevent potential collisions with track barriers. It is worth noting that in such situations, an emergency braking maneuver could jeopardize the vehicle's stability. Hence, an emergency controller must be designed to be capable of steering the vehicle while maintaining a safe distance from the track's boundaries. Vehicle path-following techniques have been extensively explored in the literature, with solutions such as loop-shaping [3], Model Predictive Control [4] [5], and learning-based methods [6]. These approaches have demonstrated promising results in autonomous racing scenarios. However, they prove to be ineffective in the event of a localization failure. This ineffectiveness stems from their reliance on precise localization information, as well as the assumption of a known reference path, i.e. not affected by uncertainty. In [7], the authors propose a wall-following algorithm as a resilient emergency solution that utilizes LiDAR sensors when GPS data becomes unreliable. In this paper, we introduce a collision avoidance controller (Fig. 2) relying on RADAR measurements, which serve to detect the position of the walls along the track boundaries. By leveraging a Total Least Squares fitting approach to construct a quadratic model from RADAR data, we derive estimates for the relative position, orientation, and curvature of the track barrier (Section II). These estimates, are fed into a Linear-Quadratic-Regulator (LQR)[8], primarily responsible for controlling the vehicle's lateral dynamics. The resulting system aims at stabilizing the racing car at a dynamically computed target distance from the wall. The controller is proven to steer the vehicle toward the barrier, thereby enhancing the fitting accuracy and reducing the distance to the wall until it reaches a value determined by the desired confidence level. Such a distance setpoint calculation yields to a nonlinear closed-loop dynamics, whose stability is analyzed

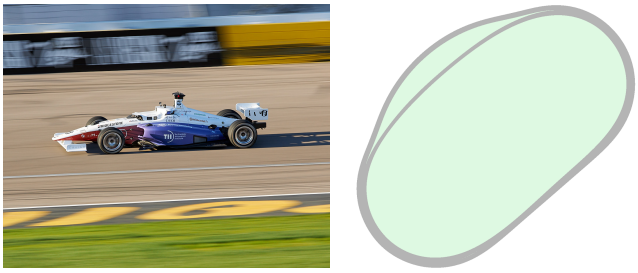

Fig. 1. Dallara AV-21 of TII Unimore Racing team and map of the Las Vegas Motor Speedway (LVMS).

Francesco Prignoli is with the Department of Electrical, Electronic, and Information Engineering "Guglielmo Marconi", Università di Bologna, Italy francesco.prignoli@unibo.it

Francesco Prignoli and Paolo Falcone are with Dipartimento di Ingegneria "Enzo Ferrari", Universita di Modena e Reggio Emilia, Italy {francesco.prignoli,paolo.falcone}@unimore.it

Paolo Falcone is with the Electrical Engineering Department, Chalmers University of Technology, Gothenburg, Sweden falcone@chalmers.se

Ayoub Raji and Marko Bertogna are with Dipartimento di Scienze Fisiche, Informatiche e Matematiche, Universita di Modena e Reggio Emilia, Italy {ayoub.raji,marko.bertogna}@unimore.it

[1] https://www.indyautonomouschallenge.com/

Copyright ©2024 EUCA

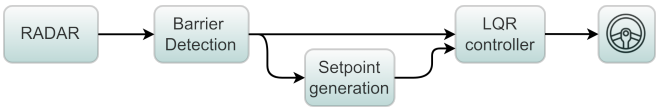

Fig. 2. RADAR-Based Emergency Controller block diagram.

in Section III. In the rest of the paper, we will use the oval track of Las Vegas Motor Speedway (LVMS) as our reference (Fig. 1), with the support of the data collected during the *Indy Autonomous Challenge @CES 2023*. Eventually, we show the results of a closed-loop simulation of the emergency controller, including the barrier detection, setpoint generation and tracking (Section IV).

II. BARRIER DETECTION

The RADAR sensor consistently demonstrates its reliability, even in high-speed scenarios. In comparison to LiDAR, RADAR provides a notably lower data point count. Nevertheless, even with such reduced data density, it remains highly effective in detecting the presence of track barriers. This characteristic not only simplifies data processing but also permits the utilization of lightweight fitting algorithms. This contrasts with LiDAR's reliance on clustering and segmentation [9], or necessitates fusion with camera sensors [10]. Consequently, RADAR emerges as a versatile and efficient sensor choice for these safety-critical applications.

It's important to note that, in our specific case, the RADAR sensor provides two distinct Field-Of-View options with varying ranges (Fig. 3). To best serve our purpose, we begin by filtering out long-range measurements, as they hold less significance for wall detection and have shown greater susceptibility to outliers. Furthermore, without loss of generality, we will focus on wall detection on the right-hand side only, according to the layout of the LVMS.

A. RADAR measurements fitting

To extract the positions of the barriers, a Least Squares fitting algorithm has been chosen. The data from the RADAR are fitted with a quadratic polynomial model; this choice has proven to be a good trade-off between accuracy in modeling the barriers profile within the selected range, given the slowly varying curvature, and robustness, avoiding an over-fitting that may affect higher-order polynomial models. It is worth noting that addressing outlier robustness requires data pre-processing and potentially incorporating robust fitting techniques, such as re-weighted least squares [11], which goes beyond this paper's scope.

The problem of fitting data that are affected by noise in both variables is described by the errors-in-variables model [12]. We assume that the pairs $(\tilde{x}_i, \tilde{y}_i),\ i = 1, \dots, m$ representing m RADAR detections in the vehicle's local coordinate frame, are subject to noise with independent Gaussian distribution, zero mean and variance $\sigma^2_{x_i} = \sigma^2_{y_i} = \sigma^2$. Our objective is to minimize the Sum of Squared Residual (SSR)

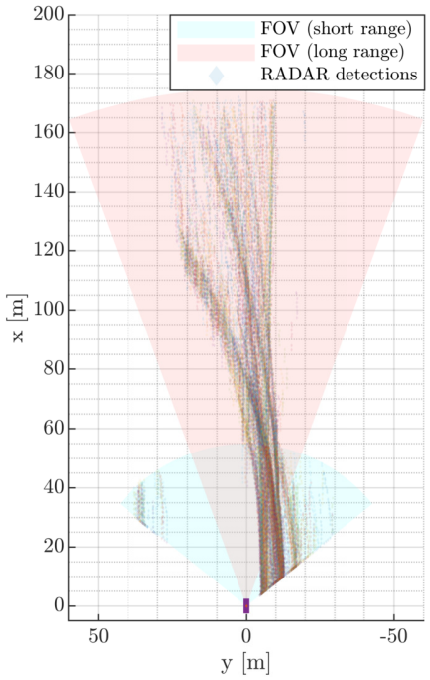

Fig. 3. RADAR detections over a full lap at LVMS during *IAC @CES 2023*.

for both the observations $\tilde{y}_i$ and $\tilde{x}_i$:

$$SSR = \sum_{i=1}^{m} (\tilde{y}_i - y_i)^2 + (\tilde{x}_i - x_i)^2 \tag{1}$$

where y_i and x_i are the true (unknown) values. Given the feature vector $\mathcal{X}_i = \mathcal{X}_i(x_i) \in \mathbb{R}^n$, we aim at determining the parameter vector β and x_i that minimize (1) when $y_i = \mathcal{X}_i^\top \beta$. Thus, we solve a Total Least Square (TLS) [13] problem that can be written as

$$\begin{aligned} &\min_{\beta, \Delta X, \Delta Y} \|[\Delta X \ \Delta Y]\|_F, \\ &\text{subj. to} \quad Y + \Delta Y = (X + \Delta X)\beta, \end{aligned} \tag{2}$$

where:

$\beta \in \mathbb{R}^n$ - Parameter vector to be estimated,
$X \in \mathbb{R}^{m \times n}$ - Design matrix of feature vectors,
$Y \in \mathbb{R}^n$ - Vector of observations y_i,
$\Delta X \in \mathbb{R}^{m \times n}$ - Correction matrix on X,
$\Delta Y \in \mathbb{R}^n$ - Correction vector on Y,
$\| \cdot \|_F$ - Frobenius norm operator.

Assuming that X is full rank, the optimization problem (2) has analytical solution for the parameter vector $\hat{\beta}$ which best fits the data in TLS sense [14]:

$$\hat{\beta} = (X^\top X - \sigma^2_{n+1} I_n)^{-1} X^\top Y. \tag{3}$$

Here, σ_{n+1} denotes the smallest singular value of the extended matrix $[X\ Y]$ and $I_n \in \mathbb{R}^n$ is the identity matrix. In our case, the rows of the design matrix X, i.e. the feature

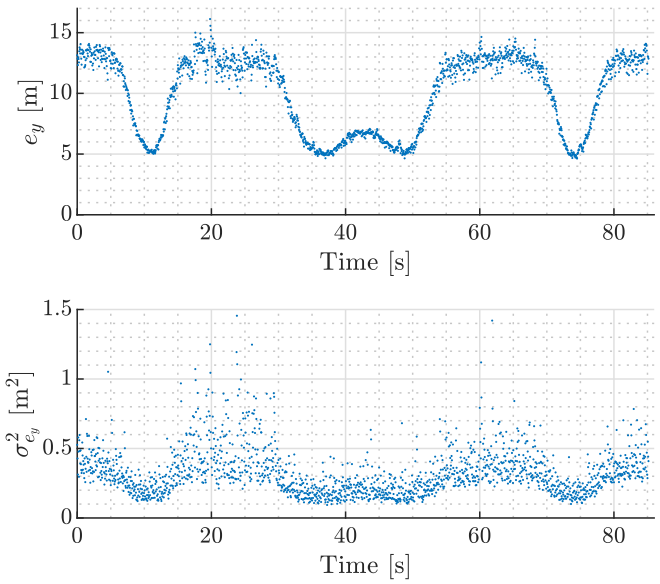

Fig. 4. Barrier distance estimate e_y and variance $\sigma^2_{e_y}$ from TLS fitting of RADAR data over a full lap at LVMS.

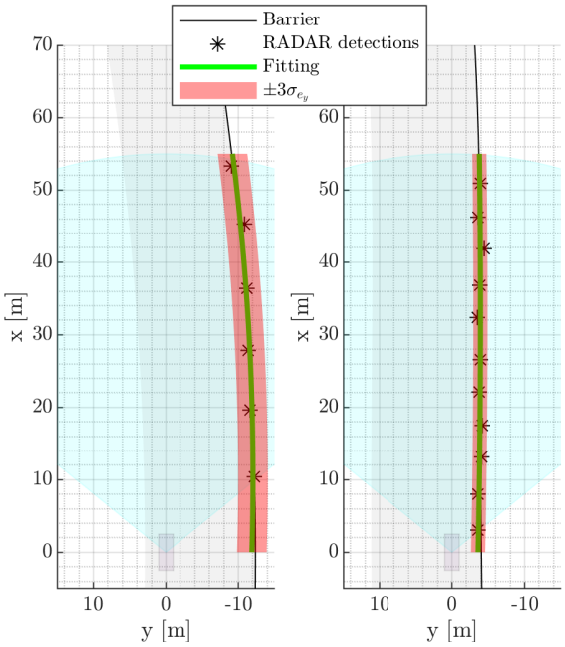

Fig. 5. Comparison of fitting from different distances to the wall.

vectors, can be expressed as $\mathcal{X}_i^\top = \begin{bmatrix} x_i^2 & x_i & 1 \end{bmatrix}$. The result is a quadratic polynomial model $y = \hat{\beta}_2 x^2 + \hat{\beta}_1 x + \hat{\beta}_0$ describing the x-y position of the barrier in the local vehicle reference frame; thus, it is possible to directly compute the current signed distance from the wall e_y, relative heading e_ψ and curvature ρ as follows:

$$e_y = -\hat{\beta}_0 \tag{4}$$

$$e_\psi = -\tan^{-1}(\hat{\beta}_1) \tag{5}$$

$$\rho = \frac{2\hat{\beta}_2}{(1+\hat{\beta}_1^2)^{\frac{3}{2}}} \tag{6}$$

Eventually, we obtain the covariance matrix for the estimated parameter vector through error propagation [15]:

$$\hat{\Sigma}_\beta = \sigma^2 (X^\top X - \sigma^2_{n+1} I_n)^{-1} \tag{7}$$

B. Setpoint generation

In the event of a loss of localization, the car must come to a safe stop at the road side while avoiding collision with the track barrier. This objective is accomplished by tracking a specific safety target distance relative to the wall. Interestingly, it becomes evident that the confidence in the estimated barrier distance (i.e. the fitting variance on the y-intercept $\hat{\beta}_0$) is closely tied to the distance itself. More in detail, the confidence level increases, meaning that the variance decreases, as the car draws closer to the wall (Fig. 4). This behavior finds its explanation in the fact that the number of RADAR data points residing on the barrier, and subsequently employed in the Total Least Squares (TLS) fitting, grows as the car approaches the wall (Fig. 5). Therefore, the target distance $e_{y,t}$ can be designed as

$$\begin{aligned} e_{y,t} &= e_{y,safe} + 3\sigma_{e_y} \\ &= f(e_y) \end{aligned} \tag{8}$$

where $e_{y,safe}$ represents the desired safety distance, σ_{e_y} stands for the standard deviation of the wall distance estimate, and $3\sigma_{e_y}$ is the 99.73% confidence interval. By shaping the target distance as in (8) we ensure that:

$$\Pr(e_{y,t} > e_{y,safe}) \simeq 99.73\% \tag{9}$$

The resulting target distance function $e_{y,t} = f(e_y)$ does not have an analytical expression, as σ_{e_y} is the result of a numerical procedure, yet the following properties:

$$\begin{cases} e_y < f(e_y) \leq e_y^* & \text{if } e_y \leq e_y^*, \\ e_y^* \leq f(e_y) < e_y & \text{if } e_y > e_y^*, \\ \dfrac{\partial f}{\partial e_y} \geq 0 & \forall e_y, \end{cases} \tag{10}$$

can be retrieved from experimental data, as showed in Fig. 6, where e_y^* represents the fixed point for f, i.e. $f(e_y^*) = e_y^*$, and it is, in general, a priori unknown.

III. LATERAL DYNAMICS CONTROL

In this section, we show how the lateral and yaw vehicle dynamics are controlled by a LQR, such that the vehicle safely approaches the roadside barriers. The dynamics of the lateral and heading error with respect to the barrier can be described by the following LPV model [16]:

$$\dot{x} = A(v)x + B_u u + B_d(v)d, \tag{11}$$

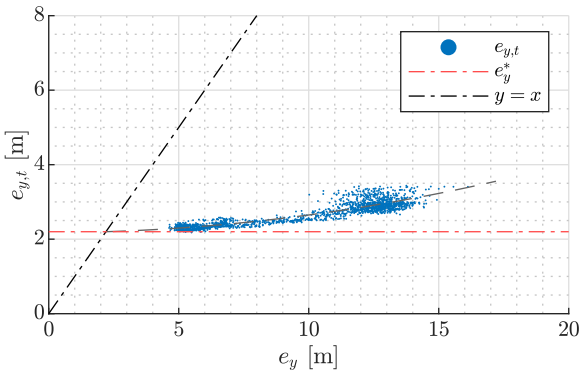

Fig. 6. Reconstruction of the target barrier distance $e_{y,t} = f(e_y)$ from data collected at LVMS. Here, $e_{y,safe} = 1$ [m]. The gray dashed line provides an illustrative representation of a potential trend for f.

where, the state, input and disturbance vectors are defined as:

$$x = \begin{bmatrix} e_y & \dot{e}_y & e_\psi & \dot{e}_\psi \end{bmatrix}^\top$$
$$u = \delta$$
$$d = \begin{bmatrix} \dot{\psi}_{bar} & \sin(\theta) \end{bmatrix}^\top$$

e_y, e_{psi} - Lateral and heading errors

δ - Front wheel angle

$\dot{\psi}_{bar}$ - "Yaw rate" of the barrier profile: $\dot{\psi}_{bar} = v\rho$

θ - Banking angle

while the matrices A, B_u, B_d are reported in Appendix (27). Although these matrices depend on the vehicle's longitudinal speed v, for the sake of clarity, we omit this dependence and will address how the proposed results can be extended to varying velocities in Section IV.

A. State-feedback control

Consider the following feedback/feed-forward control structure

$$u = -Kx + u_{ff}, \tag{12}$$

with the control gain K designed to minimize the following quadratic cost function over an infinite time horizon:

$$J = \int_0^\infty \left(x^T Q x + u^T R u\right) dt, \tag{13}$$

where $Q \succcurlyeq 0$, $R \succ 0$ are weighting penalizing the deviation of the state and input vector from the origins of the state and input spaces, respectively. Under the assumption that the pair (A, B_u) is stabilizable, the control gain K, which minimizes the cost (13) subject to the model (11), is the solution of the infinte-time Linear Quadratic Regulator (LQR) problem:

$$K = R^{-1} B^T P \tag{14}$$

where P is the symmetric positive definite solution of the continuous-time algebraic Riccati equation (CARE):

$$A^T P + PA - (PB)R^{-1}(B^T P) + Q = 0 \tag{15}$$

The feed-forward input u_{ff} is designed such that the tracking error $\epsilon_y = e_y - e_{y,t}$, where $e_{y,t}$ is the target distance from the barrier calculated as in (8), is zero at steady state. Thus, u_{ff} is found as solution of the linear system of equations

$$\mathbf{0} = (A - B_u K)x_t + B_u u_{ff} + B_d d \tag{16}$$

where x_t denotes the target setpoint. It can be shown that, in this case, the target setpoint $x_t = \begin{bmatrix} e_{y,t} & 0 & e_{\psi,t} & 0 \end{bmatrix}^\top$ is a solution of (16), wherein we adopt $e_{y,t} = f(e_y)$ as in (8), while $e_{\psi,t}$ is determined by (16) and it depends (linearly) on the disturbance $\dot{\psi}_{bar}$ only. The closed-loop dynamics resulting from (12) and (16) are

$$\dot{x} = (A - B_u K)(x - x_t) = A_{CL}(x - x_t), \tag{17}$$

where we introduced $A_{CL} \triangleq A - B_u K$.

It is important to note that, according to (8), the target state x_t in (17) is a not completely known nonlinear function of the system state x. Indeed, while the properties outlined in (10) are known to hold for the function f, the analytical expression of this function is unavailable. Hence, the stability of (17) is to be studied through Lyapunov stability analysis tools.

B. Closed-loop stability analysis

Let us introduce the change of variables $z \triangleq x - x_t^*$, where $x_t^* = \begin{bmatrix} e_y^* & 0 & e_{\psi,t} & 0 \end{bmatrix}^\top$ is the constant setpoint, generally unknown, that is solution of (16) when $e_{y,t} \equiv e_y^*$. Consequently, the closed-loop dynamics can be expressed in terms of z as:

$$\dot{z} = \dot{x} - \cancel{\dot{x}_t^*} = A_{CL}(z + x_t^* - x_t) = A_{CL}(z - z_t), \tag{18}$$

where $z_t \triangleq x_t - x_t^* = \begin{bmatrix} (e_{y,t} - e_y^*) & 0 & 0 & 0 \end{bmatrix}^\top$.

Theorem 1 (Sufficient stability condition): Define the matrices:

$$M \triangleq \begin{bmatrix} \alpha(z) & 0 & 0 & 0 \\ 0 & 0 & 0 & 0 \\ 0 & 0 & 0 & 0 \\ 0 & 0 & 0 & 0 \end{bmatrix} \mid z_t = Mz, \tag{19}$$

$$\bar{M} \triangleq I - M, \tag{20}$$

with I the identity matrix and:

$$\alpha(z) = \begin{cases} 0, & \text{if } e_y = e_y^* \\ \dfrac{z_{t,1}}{z_1} = \dfrac{e_{y,t} - e_y^*}{e_y - e_y^*} & \text{if } e_y \neq e_y^*, \end{cases} \tag{21}$$

where the subscript 1 indicates the first component of the vectors z_t and z. The properties introduced in (10) yields:

$$\alpha(z) \in [0, 1), \quad \forall z. \tag{22}$$

Given a control gain K, if the matrix $A_{CL}\bar{M}$ is Hurwitz $\forall \alpha \in [0, 1)$, then the state x of the closed-loop system (17) converges to x_t^* as $t \to \infty$.

Proof: Consider the candidate Lyapunov function $V(z) = z^\top P z$, $P \succ 0$. Its time derivative along the trajectories of the closed-loop system is

$$\begin{aligned} \dot{V}(z) &= z^\top P \dot{z} + \dot{z}^\top P z \\ &= z^\top P(A_{CL}(z - z_t)) + (A_{CL}(z - z_t))^\top P z, \end{aligned} \tag{23}$$

Substituting (19) and (20) into (23) yields:

$$\begin{aligned}\dot{V}(z) &= z^\top P(A_{CL}(z - Mz)) + (A_{CL}(z - Mz))^\top Pz \\ &= z^\top P(A_{CL}\bar{M}z) + (A_{CL}\bar{M}z)^\top Pz \\ &= z^\top (P(A_{CL}\bar{M}) + (A_{CL}\bar{M})^\top P)z.\end{aligned} \tag{24}$$

By the Lyapunov theorem [17], if the matrix $A_{CL}\bar{M}$ is Hurwitz, there exists a positive definite matrix Q satisfying the Lyapunov equation:

$$P(A_{CL}\bar{M}) + (A_{CL}\bar{M})^\top P = -Q, \tag{25}$$

It follows:

$$\dot{V}(z) = -z^\top Qz < 0, \ \forall \ z \neq \mathbf{0}, \tag{26}$$

that proves the asymptotic stability of the system (18). Hence, z converges to the origin, implying that x converges to x_t^* as $t \to \infty$. ■

While studying the stability property of the matrix $A_{CL}\bar{M}$ as $\alpha(z) \in [0, 1)$ is not straightforward, Fig. 7 illustrates how the eigenvalues of $A_{CL}\bar{M}$ move in the complex plane as $\alpha(z)$ varies. For the sake of readability, only the eigenvalues closest to the imaginary axis are shown. While for $\alpha = 0$ we obtain the case $z_t = \mathbf{0}$ (i.e. $e_{y,t} \equiv e_y^*$) and closed-loop stability holds, for $\alpha > 1$ the system becomes unstable as the target distance $e_{y,t}$ exceeds the current vehicle distance from the barrier, i.e. the target z_t does not align with the origin. An alternative interpretation of this result is to consider that α represents the rate of increase in the standard deviation of the wall distance estimate, with the distance itself. When $\alpha = 0$, $\bar{M}$ transforms into the identity matrix, ensuring the system's inherent stability due to the design of A_{CL}. Consequently, in general, it is reasonable to anticipate the existence of an upper limit, denoted as α_{max}, falling within the interval $(0, 1]$, and such that the system is stable for $\alpha \in [0, \alpha_{max})$. Notably, the value of α_{max} is intrinsically linked to the performance of the RADAR sensor and of the detection algorithm in terms of accuracy of the wall distance estimate, essentially setting a minimum requirement for guaranteeing system stability.

IV. SIMULATION RESULTS

The emergency controller pipeline (Fig. 2) has been designed and simulated within the Matlab & Simulink environment. The vehicle model used for closed-loop simulation consists in a double-track vehicle model, properly parameterized according to the AV-21 specifications. The barrier detection module takes (synthetic) RADAR data as input and furnishes estimates of barrier distance, orientation, and curvature, along with their respective variances. The extracted measurements are then utilized to construct the target wall distance and to estimate the controller's state via a Kalman filter. It's worth noting that, for the sake of comprehensiveness, we mention that the proposed design can be seamlessly extended to the discrete-time domain, which is commonly employed in practical controller deployment. As previously stated, the system (11) is LPV due to the speed-dependent matrices. A control gain-scheduling, speed-dependent approach [18] can be used, provided that the stability condition in Section III is imposed as well. Figure 8 shows the results of a closed-loop simulation conducted on the LVMS track. The vehicle is traveling at 200 kph while maintaining a distance of approximately 12 meters from the barrier. At $t = 5$ seconds, a localization failure triggers the emergency controller. The latter starts tracking the target distance, which gradually decreases as the car approaches the barrier, ultimately stabilizing around a value e_y^*. Simultaneously, the confidence level in the distance estimate improves, that is the estimation covariance decreases and reaches its minimum at $e_y = e_y^*$. As a result, the car smoothly decelerates and safely comes to a halt, all while ensuring a secure distance is maintained from the barrier.

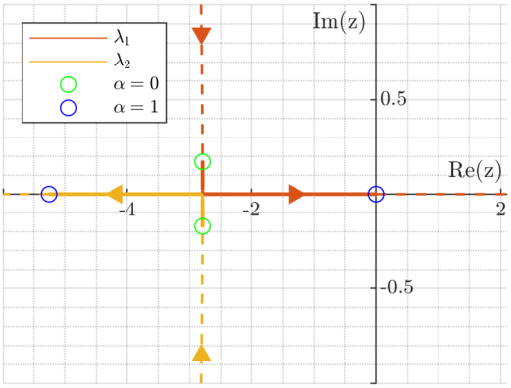

Fig. 7. Eigenvalues λ_i of $A_{CL}\bar{M}$ closest to the instability region as function of α. The arrows indicate the direction of increasing α. The dashed lines denote the eigenvalues for $\alpha \notin [0, 1)$.

V. CONCLUSIONS

We have presented a LQR controller for lateral dynamics, specifically designed to safely approach the track barriers, using only RADAR data, in scenarios that lack precise localization. Our approach incorporates a Total Least Square method that fits a quadratic polynomial model to the RADAR data of the barriers position. The lateral controller is made aware of the uncertainty of the estimated distance to the barriers by providing the LQR controller with a target distance that encompasses the "three-sigma" confidence interval. The stability of the resulting closed-loop dynamics, which is *nonlinear*, has been studied using the Lyapunov stability theory. The obtained sufficient stability conditions allow checking that the designed controller leads to a fixed point distance to the barriers. Finally, we have successfully deployed and simulated the entire system, demonstrating the consistency of our anticipated results. This comprehensive work contributes valuable insights and a functional solution for enhanced safety and control in autonomous racing car scenarios, setting the stage for further advancements in this field. For completeness, a robustness analysis should be provided to further validate the system's performance under varying conditions and uncertainties. Current limitations include the absence of

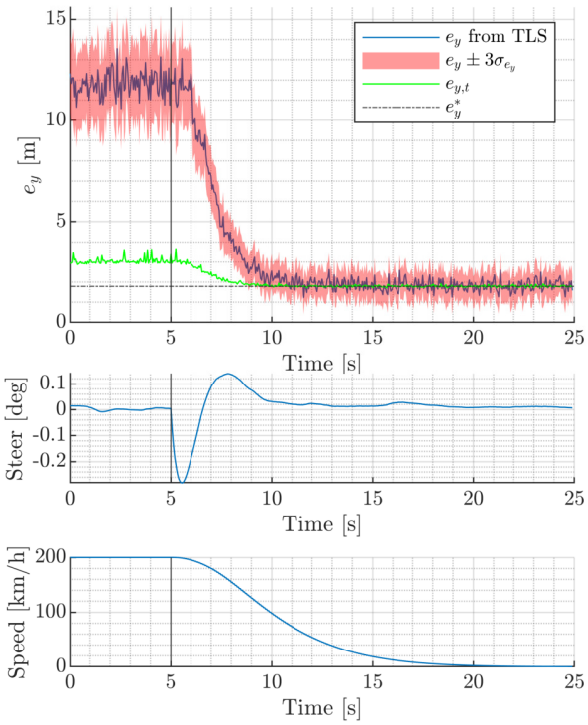

Fig. 8. Closed-loop simulation. At time $t = 5$ seconds, a localization failure triggers the emergency controller, which starts tracking the target distance $e_{y,t}$ while the vehicle smoothly decelerates.

considerations for other vehicles. A potential strategy could involve adjusting the target distance to the barrier to create a trajectory that avoids obstacles. As part of our future work, we plan to conduct preliminary field tests on a passenger car before progressing to experiments with the AV-21.

APPENDIX

$$A = \begin{bmatrix} 0 & 1 & 0 & 0 \\ 0 & -\frac{C_f + C_r}{mv} & \frac{C_f + C_r}{m} & \frac{-C_f l_f + C_r l_r}{mv} \\ 0 & 0 & 0 & 1 \\ 0 & -\frac{C_f l_f - C_r l_r}{I_z v} & \frac{C_f l_f - C_r l_r}{I_z} & -\frac{C_f l_f^2 + C_r l_r^2}{I_z v} \end{bmatrix}$$

$$B_u = \begin{bmatrix} 0 \\ \frac{C_f}{m} \\ 0 \\ \frac{C_f l_f}{I_z} \end{bmatrix} \quad B_d = \begin{bmatrix} 0 & 0 \\ -\frac{C_f l_f - C_r l_r}{mv} - v & g \\ 0 & 0 \\ -\frac{C_f l_f^2 + C_r l_r^2}{I_z v} & 0 \end{bmatrix}$$

v - Vehicle speed
C_f, C_r - Front and rear tire cornering stiffness
l_f, l_r - Front and rear axle distance from the CoG
m, Iz - Vehicle mass and inertia
g - Gravitational acceleration

(27)

ACKNOWLEDGMENT

We extend our heartfelt thanks to the members of the TII Unimore Racing team for their invaluable support in advancing this work.

REFERENCES

[1] J. Betz, *et al.*, "TUM autonomous motorsport: An autonomous racing software for the Indy Autonomous Challenge," *Journal of Field Robotics*, vol. 40, no. 4, pp. 783–809, June 2023.
[2] A. Wischnewski, T. Stahl, J. Betz, and B. Lohmann, "Vehicle Dynamics State Estimation and Localization for High Performance Race Cars," *IFAC-PapersOnLine*, vol. 52, no. 8, pp. 154–161, 2019.
[3] M. Corno, *et al.*, "A Non-Optimization-Based Dynamic Path Planning for Autonomous Obstacle Avoidance," *IEEE Transactions on Control Systems Technology*, vol. 31, no. 2, pp. 722–734, Mar. 2023.
[4] A. Wischnewski, T. Herrmann, F. Werner, and B. Lohmann, "A Tube-MPC Approach to Autonomous Multi-Vehicle Racing on High-Speed Ovals," *IEEE Transactions on Intelligent Vehicles*, vol. 8, no. 1, pp. 368–378, Jan. 2023.
[5] A. Raji, *et al.*, "Motion Planning and Control for Multi Vehicle Autonomous Racing at High Speeds," in *2022 IEEE 25th International Conference on Intelligent Transportation Systems (ITSC)*. Macau, China: IEEE, Oct. 2022, pp. 2775–2782.
[6] U. Rosolia and F. Borrelli, "Learning How to Autonomously Race a Car: A Predictive Control Approach," *IEEE Transactions on Control Systems Technology*, vol. 28, no. 6, pp. 2713–2719, Nov. 2020.
[7] D. Lee, C. Jung, A. Finazzi, H. Seong, and D. H. Shim, "A resilient navigation and path planning system for high-speed autonomous race car," 2022.
[8] B. D. Anderson and J. B. Moore, *Optimal control: linear quadratic methods*, ser. Prentice Hall information and system sciences series. Englewood Cliffs, N.J: Prentice Hall, 1989.
[9] R. Qian, X. Lai, and X. Li, "3D Object Detection for Autonomous Driving: A Survey," *Pattern Recognition*, vol. 130, p. 108796, Oct. 2022.
[10] X. Zhao, P. Sun, Z. Xu, H. Min, and H. Yu, "Fusion of 3D LIDAR and Camera Data for Object Detection in Autonomous Vehicle Applications," *IEEE Sensors Journal*, vol. 20, no. 9, pp. 4901–4913, May 2020.
[11] I. Daubechies, R. DeVore, M. Fornasier, and C. S. Güntürk, "Iteratively reweighted least squares minimization for sparse recovery," *Communications on Pure and Applied Mathematics*, vol. 63, no. 1, pp. 1–38, Jan. 2010.
[12] S. Van Huffel and P. Lemmerling, Eds., *Total Least Squares and Errors-in-Variables Modeling: Analysis, Algorithms and Applications*. Dordrecht: Springer Netherlands, 2002.
[13] I. Markovsky and S. Van Huffel, "Overview of total least-squares methods," *Signal Processing*, vol. 87, no. 10, pp. 2283–2302, Oct. 2007.
[14] I. Hnětynková, M. Plešinger, D. M. Sima, Z. Strakoš, and S. Van Huffel, "The Total Least Squares Problem in AXB: A New Classification with the Relationship to the Classical Works," *SIAM Journal on Matrix Analysis and Applications*, vol. 32, no. 3, pp. 748–770, July 2011.
[15] D. C. Montgomery, E. A. Peck, and G. G. Vining, *Introduction to linear regression analysis*, 5th ed., ser. Wiley series in probability and statistics. Hoboken, NJ: Wiley, 2012, no. 821.
[16] R. Rajamani, *Vehicle Dynamics and Control*, ser. Mechanical Engineering Series. Boston, MA: Springer US, 2012.
[17] N. P. Bhatia and G. P. Szego, *Stability theory of dynamical systems*, ser. Classics in mathematics. Berlin ; New York: Springer, 2002.
[18] R. Rajamani, "Steering Control for Automated Lane Keeping," in *Vehicle Dynamics and Control*. Boston, MA: Springer US, 2012, pp. 47–85.